J Neurophysiol 89: 2854–2867, 2003;
10.1152/jn.01051.2002.

report

Morphological and Physiological Characterization of Layer VI Corticofugal Neurons of Mouse Primary Visual Cortex

Joshua C. Brumberg, Farid Hamzei-Sichani, and Rafael Yuste
Department of Biological Sciences, Columbia University, New York, New York 10027

Submitted 22 November 2002; accepted in final form 2 January 2003

Brumberg, Joshua C., Farid Hamzei-Sichani, and Rafael Yuste. Morphological and physiological characterization of layer VI corticofugal neurons of mouse primary visual cortex. *J Neurophysiol* 89: 2854–2867, 2003; 10.1152/jn.01051.2002. Layer VI is the origin of the massive feedback connection from the cortex to the thalamus, yet its complement of cell types and their connections is poorly understood. The physiological and morphological properties of corticofugal neurons of layer VI of mouse primary visual cortex were investigated in slices loaded with the Ca^{2+} indicator fura-2AM. To identify corticofugal neurons, electrical stimulation of the white matter (WM) was done in conjunction with calcium imaging to detect neurons that responded with changes in intracellular Ca^{2+} concentrations in response to the stimulation. Subsequent whole cell recordings confirmed that they discharged antidromic action potentials after WM stimulation. Antidromically activated neurons were more excitable and had different spiking properties than neighboring nonantidromic neurons, although both groups had similar input resistances. Furthermore, antidromic neurons possessed narrower action potentials and smaller afterhyperpolarizations. Additionally, three-dimensional reconstructions indicated that antidromically activated neurons had a distinct morphology with longer apical dendrites and fewer nonprimary dendrites than nonantidromic cells. To identify the antidromic neurons, rhodamine microspheres were injected into the dorsal lateral geniculate nucleus of the thalamus and allowed to retrogradely transport back to the somata of the layer VI cortico-geniculate neurons. Physiological and anatomical analysis indicated that most antidromic neurons were likely to be cortico-geniculate neurons. Our results show that cortico-thalamic neurons represent a specific functional and morphological class of layer VI neurons.

INTRODUCTION

The neocortex can be divided into six distinct layers based on cell density (Lorente de Nó 1949). Each lamina is composed of distinct classes of neurons that are believed to subserve different processing roles (for review, see Mountcastle 1998). Layer IV serves as the main target of thalamocortical axons and is populated by excitatory cells such as small pyramidal neurons and spiny stellate cells and several classes of interneurons (White 1989). The main output of the cortex is via the infragranular layers, layers 5 and 6 (Jones 1984). There has been extensive studies of the morphology, physiology, and connectivity of layer V (e.g., Kozloski et al. 2001; Markram et al. 1997), but less work has focused on layer VI. Layer VI is the origin of the major feedback connection to the sensory thalamus (Jones 1984) as well as another target of thalamocortical axons (Chmielowska et al. 1989). Layer VI feedback to the thalamus has a strong influence on the firing properties of thalamocortical relay cells (for review, see Guillery and Sherman 2002; Sherman and Guillery 1998). Despite its potentially crucial role in regulating thalamocortical interactions, relatively less attention has been focused on the physiological properties of the neurons in layer VI.

Anatomically, layer VI is very diverse (Prieto and Winer 1999; Tombol 1984). Previous reports have used largely qualitative comparisons to distinguish between different cell types (see Ferrer et al. 1986a,b). One class of layer VI neurons is the corticothalamic pyramidal cells that tend to reside in the upper half of layer VI (Zhang and Deschenes 1997). Corticothalamic neurons receive direct thalamic input (White and Hersch 1982) and in turn project both to layer IV and the thalamus (Burkhalter 1989; Staiger et al. 1996; Usrey and Fitzpatrick 1996). Within the thalamus, the number of feedback connections from the cortex vastly exceeds the number of feedforward inputs from the sensory periphery (Erisir et al. 1997). Thus corticothalamic neurons are hypothesized to play a pivotal role in gating the sensory information that reaches the cortex via this feedback connection (Sherman and Guillery 1998).

Previous in vitro electrophysiological studies in layer VI have found qualitative differences between neurons (see Yang et al. 1996). For instance, differences in adaptive properties (van Brederode and Snyder 1992) and afterhyperpolarizations (Kang and Kayano 1994) have been noted, but no attempts have been made to relate these differences to functional classes such as cortico-thalamic versus local circuit neurons. In the present study, a combined optical and physiological approach was taken to identify and characterize a specific class of corticofugal neurons in layer VI of the primary visual cortex (V1) of the juvenile mouse.

METHODS

Preparation of slices

Acute coronal slices of primary visual cortex (300 μm thick) were prepared from postnatal days 11 to 18, C57BL/6 mice of either sex on a vibratome (VT1000s, Leica) in accordance with Columbia University and National Institutes of Health (NIH) guidelines for the use of animals in biomedical experiments. Mice were anesthetized with an injection (0.1 ml ip) of a mixture of ketamine (2.5 g/50 ml dH_20)/xylazine (0.125 g/50 ml dH_20). When the mouse became unrespon-

Present address and address for reprint requests: J. C. Brumberg, Dept. of Psychology, Queens College, 65-30 Kissena Bld., Flushing, NY 11367 (E-mail: joshua_brumberg@qc.edu).

The costs of publication of this article were defrayed in part by the payment of page charges. The article must therefore be hereby marked "*advertisement*" in accordance with 18 U.S.C. Section 1734 solely to indicate this fact.

sive to noxious stimulus, a toe pinch, the mouse was decapitated and the brain quickly removed, blocked, and placed into ice-cold (4°C) oxygenated artificial cerebral spinal fluid (ACSF). ACSF contained (in mM) 124 NaCl, 2.5 KCl, 2 $MgSO_4$, 1.25 NaH_2PO_4, 1.2 $CaCl_2$, 26 $NaHCO_3$, and 10 dextrose and was aerated with 95% O_2-5% CO_2 to a final pH of 7.4. Slices were allowed to recover for 1 h at room temperature before bulk loading with the calcium indicator Fura-2AM.

Calcium imaging

We used a modification of the procedure utilized by Yuste and Katz (1991) for bulk loading the slices. Briefly, the slices were incubated at room temperature in the dark for 45–60 min in a small petri dish containing ~3 ml of oxygenated ACSF and 50 μl of 50μM Fura-2AM (Molecular Probes) in DMSO (Sigma). After the loading, the slices were transferred to a bath of oxygenated ACSF at room temperature for 15 min prior to the initiation of the experiment.

Ca^{2+} imaging was conducted on an upright Olympus BX50WI microscope with a ×40 (0.8 NA) water-immersion objective (Olympus). We used a 380-nm excitation filter, a 395-nm dichroic mirror, and a 510-nm emission filter (Chroma). Changes in fluorescence were captured using a SIT camera (C-2400, Hamamatsu) and digitized with a Scion Image frame grabber (LG-3, Scion) at a frame rate of 6–7 Hz using NIH Image on a Power PC (Radius). On-line analysis of the collected images was done using NIH Image. For each pixel the change in fluorescence (in %) was computed in reference to the prestimulus condition (see following text). Thus for each pixel of each frame, $\Delta F/F_o$ was computed where F_o was the resting fluorescence. The resultant movies were used to guide the electrophysiological recordings toward neurons that either did or did not have changes in their fluorescence after extracellular white matter stimulation (see Fig. 1*C*).

Electrophysiological recordings

Neurons were recorded using the whole cell patch-clamp technique in current-clamp configuration. Neurons of interest were identified by their response or lack of response to white matter stimulation in the $\Delta F/F_o$ movies and targeted using DIC optics coupled with fluorescent

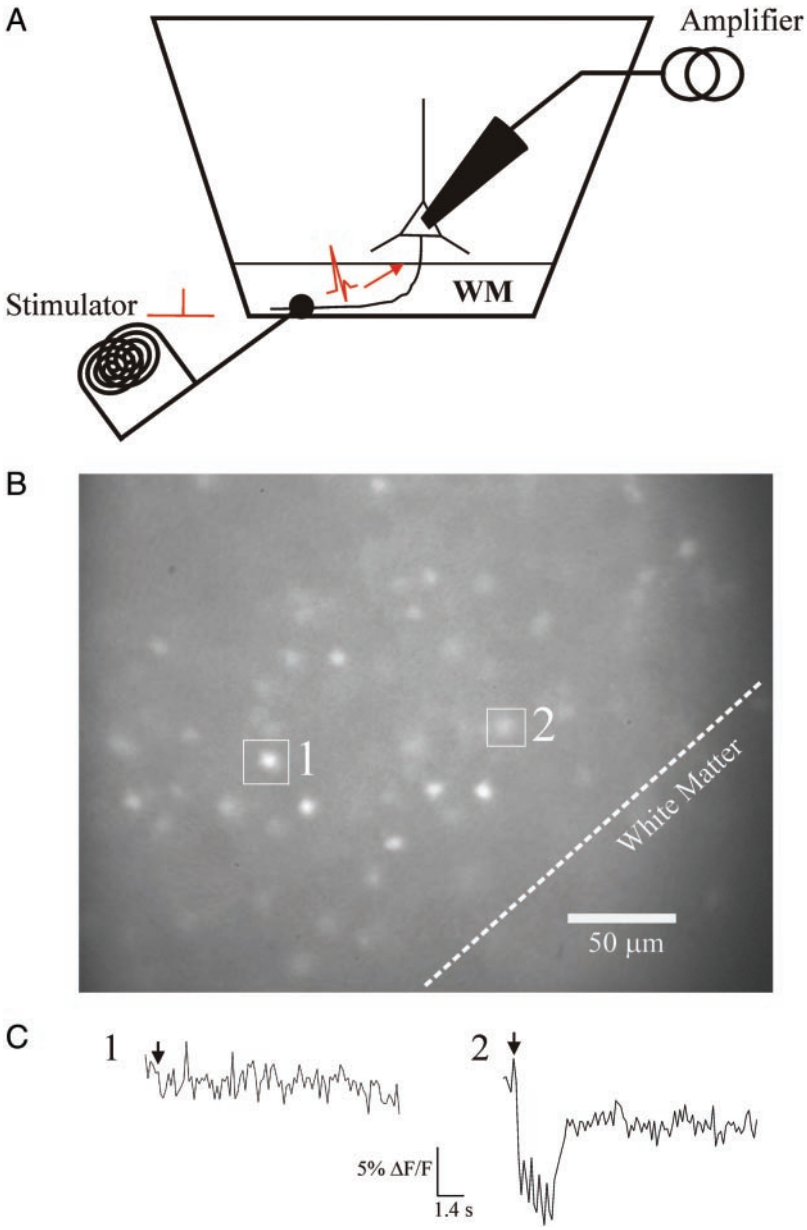

FIG. 1. Schematic of the experiment. A corticofugal neuron is antidromically activated by the tungsten stimulating electrode and an antidromic action potential travels retrogradely toward the soma (*A*). Resting levels of fluorescence after Fura-2AM bulk loading (*B*). The optical responses of neuron 1 (C*1*) and neuron 2 (C*2*) in response to 10 100-μs pulses of −0.1 mA delivered at 5 Hz. The arrows indicate the onset of the stimulus. Some neurons responded with changes ($\Delta F/F_o$) in response to the extracellular stimulation (*C2*) and some did not (*C1*).

imaging to identify the somata of the neurons to be studied. Current-clamp recordings were carried out with two Dagan amplifiers (BVC-700A, Dagan Instruments), and the data were filtered at 1 kHz and digitized at 10 kHz with a MacAdios A/D board (GW Instruments) using Superscope (GW Instruments). Liquid junction potentials and series resistance were manually compensated. Standard patch pipettes (~4–7 MΩ tip resistance) were pulled on a Flaming/Brown micro-electrode puller (P-97, Sutter Instruments). Pipettes were filled with (in mM) 130 $KMeSO_4$, 5 NaCl, 10 KCl, 10 HEPES, 2.5 Mg-ATP, 0.3 Na-GTP, and 0.3–1% biocytin (wt/vol) for subsequent visualization of the neurons (see following text). Once a stable recording had been obtained (resting V_m of –55 mV or more negative, overshooting action potentials, ability to generate repetitive spikes to a depolarizing current pulse), the cell was classified according to its discharge pattern in response to a constant depolarizing current pulse (120 ms, +0.5 nA) as intrinsically bursting, regular spiking, fast spiking, or chattering (Brumberg et al. 2000; McCormick et al. 1985). All the neurons in the present study were recorded at ~35°C and classified as regular spiking unless noted. Off-line analysis of action potential and passive membrane properties was done on a PC using the MiniAnalysis software package (Synaptosoft). Statistics were computed using the Statistica software package (StatSoft) on a PC. For between group analyses, ANOVAs were conducted; post hoc two-tailed *t*-test were used to determine the source of the variance if any. Statistical significance was achieved when $P < 0.05$ unless noted. All data, if not noted, are reported as means ± 1 SD.

Extracellular stimulation for both the imaging and physiology was done via a monopolar tungsten electrode (~1 MΩ, Fredrick Hare) attached to an Iso-flex stimulation isolation unit (AMPI) triggered by a Master-8 stimulus controller (AMPI). Typically, an experiment was initiated by the imaging computer, which opened an electronic shutter (UniBlitz, Vincent Associates) that then initiated the image collection and with a 1-s delay triggered a short train (8–10 pulses each lasting 100 μs each) at 5 Hz delivered to the white matter via the tungsten stimulating electrode (see Fig. 1*A*). At low frequencies (<10 Hz), there was no temporal summation, but at higher frequencies, somatic spikes could be activated by this feedforward input. To ensure that feedforward action potentials were not evoked, which would result in false positive identification of antidromic neurons in the calcium imaging, the stimuli were delivered at a sufficiently slow frequency (5 Hz) to minimize temporal summation of incoming postsynaptic potentials (PSPs). The magnitude of the stimulus was set at −0.1 mA, which resulted in the activation of two to three neurons based on the imaging data (see RESULTS), suggesting that we were not strongly activating the slice. If the stimulus intensity was significantly increased (>3 mA), many more neurons would respond, presumably due to orthodromic activation.

Injection of rhodamine microspheres

To positively identify cortico-geniculate neurons, rhodamine-labeled beads were injected into the dorsal lateral geniculate nucleus of the thalamus (dLGN) of Postnatal day (PND) 8–10, C57BL/6 mice of either sex. Mice were anesthetized, with an injection (0.02 ml ip) of an anesthetic mixture containing ketamine (45 mg/ml) and xylazine (5 mg/ml) dissolved in dH_20, and then placed in a stereotaxic apparatus. After a small craniectomy, rhodamine-labeled fluorescent latex microspheres (Lumafluor) were loaded into micropipettes and pressure injected stereotaxically into the dLGN based on coordinates derived experimentally (2.25 mm lateral from midline, 3.00 mm anterior to lambda, and 2.50 mm deep to the pial surface) with a picospritzer (General Valve). Mice were allowed to recover for a minimum of 3 days to ensure adequate retrograde bead transport to the visual cortex. The intensity of bead labeling did not change from 3 to 5 days postinjection. To confirm the location of the injection, coronal slices were taken from the blocked mouse brain through the level of the LGN. The slices containing the LGN were viewed at low magnification (×4 or ×10) to determine the extent of the LGN (in brightfield) and with the fluorescent light to determine the extent of the bead injection. Only mice where injections were confined to the dLGN and or the ventral LGN (vLGN) were subsequently recorded from.

Histology

After a successful recording the slice was placed immediately in ice-cold fixative (4% paraformaldehyde, 1.25% glutaraldehyde in 0.1 M phosphate buffer) and kept at 4°C for ≤2 wk. The slices were then processed for biocytin, which was included in the intracellular recording solution (see preceding text) using an ABC kit (Vector Labs). The slices were mounted on polylysine-coated slides (Sigma) quickly dehydrated and defatted and coverslipped using Entallan mounting medium (Electron Microscopy Sciences). For three-dimensional morphological reconstructions, the Neurolucida system (MicroBrightfield) was used in conjunction with an inverted Olympus IX70 microscope using a ×60 (1.40 NA) oil immersion lens (PlanApo, Olympus). Morphological measurements were made using the NeuroExplorer software package (MicroBrightfield).

RESULTS

Optical identification of antidromic neurons

Our objective was to optically identify antidromically driven cells in layer VI to subsequently characterize them anatomically and physiologically. A tungsten stimulating electrode was placed in the white matter (≥1 mm from the potential recording site; Fig. 1*A*), a train of 8–10 pulses (100 μs of −0.1 mA), was delivered at 5 Hz while imaging the slice for changes in somatic intracellular-free calcium concentration $[Ca^{2+}]_i$, as indicated by fluorescence measurements using Fura-2 (Fig. 1, *B* and *C*). The relative placement of the stimulating electrode was important: placing the electrode in the ventral aspects of the white matter resulted in more activation as judged from the calcium imaging (data not shown), consistent with the known path of the axons originating from layer VI corticothalamic neurons (Woodward and Coull 1984; Woodward et al. 1990). Thus two classes of neurons were operationally defined based on their optical signature: those that showed changes in fluorescence in response to white matter stimulation (Fig. 1*C2*) and those that did not (Fig. 1*C1*). It is expected that white matter stimulus would also activate cortico-tectal neurons in layer V, although likely, our field of view was limited by the objective only to layer VI and the underlying white matter (see Fig. 1*B*), we did not note any changes in layer V neurons.

Electrophysiological confirmation of antidromic activation

To test our hypothesis that the neurons that showed significant stimulus-evoked changes in their resting fluorescence were indeed antidromically activated, these neurons were targeted for whole cell recordings. For a neuron to be considered antidromically activated, it had to meet *all* of the following criteria: it had the ability to follow a 100-Hz stimulus without action potential failure (Fig. 2*A*), there was no change in its interspike interval (Fig. 2*A*, *inset*), and the invasion of the antidromic action potential into the soma could be prevented by the induction of a somatic spike (via current injection) at a

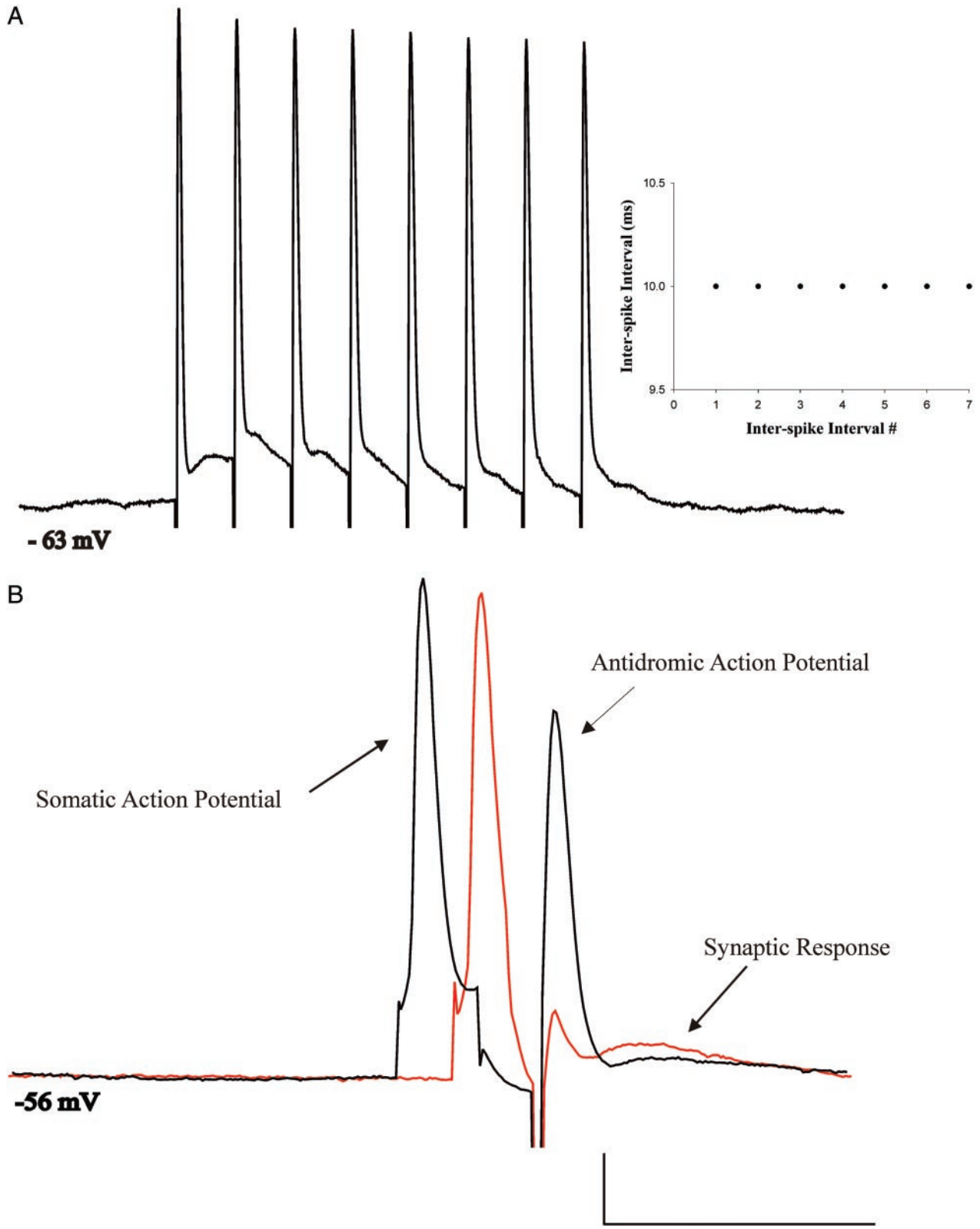

FIG. 2. Confirmation of antidromic activation. *A*: response of a neuron that was optically identified to have significant changes in $\Delta F/F_o$ after white matter stimulation to a 100-Hz stimulus. Note how the interspike interval showed no jitter (*A, inset*). *B*: a collision test confirmed the antidromic activity. Initiation of a somatic spike, 5 ms prior to white matter stimulation, did not prevent the invasion of the soma by the antidromic action potential, but initiating the somatic spike 3 ms prior to stimulation prevented antidromic invasion. Note that the synaptic input is not affected by the somatic action potential. Stimulus artifacts have been truncated. The scale bar is equivalent to 10 mV and 20 ms for *A* and 13 mV and 4.6 ms for *B*.

short enough interval (collision test; Fig. 2*B*). To minimize the duration of the somatic current injection and ensure the initiation of an action potential, short (2–3 ms), large-amplitude (5.0−8.0 nA), depolarizing pulses were used. Antidromic action potentials tend to have faster rise times than somatically induced action potentials, are less prone to failure, and are of smaller amplitude than somatically evoked action potentials (for review, see Eccles 1952). Furthermore, the mean latency to the first action potential initiated by the stimulus was <1 ms (mean = 0.84 ± 0.3 ms), which is a shorter interval than what was observed for the orthodromic activity (Fig. 2). The neuron pictured in Fig. 2 is representative of our antidromically activated neurons.

All neurons detected optically met these criteria (20 of 20) and were classified as being antidromically activated. Neurons that did not show changes in their resting fluorescence, recorded from the same slices, were subsequently found to not discharge antidromic action potentials (14 of 14). These neurons were presumably not activated due to the location of the stimulating electrode (in the ventral aspect of the white matter), the low stimulus intensity, and, as shown below, their axons did not penetrate the white mater. In the case of the antidromic neurons, however, their axons could often be traced back to the white matter. These findings confirmed our hypothesis that the changes in baseline fluorescence observed during the Ca^{2+} imaging was due to antidromic activity and validated an optical method for identifying and targeting at least one population of corticofugal neurons.

Antidromically activated neurons show less synaptic depression

In both antidromic neurons and nonantidromic neurons, synaptic inputs were activated following white matter stimulation, presumably due to feedforward afferents from the thalamus, other cortical afferents coursing through the white matter or recurrent activation of neocortical cells (Fig. 3). We wondered whether there were any differences in the synaptic responses in antidromic and nonantidromic cells. To test this, we measured the amplitude of the first and last PSP of a train evoked in response to different frequencies of white matter stimulation (8 stimuli; Fig. 3, *A* and *C*). Both classes of neurons responded similarly to the first stimulus (16.8 ± 10.4 mV for antidromic neurons, $n = 20$ vs. 16.8 ± 11.2 mV for nonantidromic neurons, $n = 14$) and showed synaptic depression; responses to the eighth stimuli were significantly depressed when compared with the first stimulus (Fig. 3*B*, paired *t*-test, $P < 0.004$; response to the 8th stimuli was 14.69 ± 9.67 mV for the antidromic neurons and 11.36 ± 9.32 mV for the nonantidromic neurons). Interestingly, the depression observed in the nonantidromically activated neurons was greater than that seen in the antidromically activated neurons (Fig. 3*D*; ratio of 8th response to the 1st of antidromic neurons 0.86 ± 0.16 vs. 0.55 ± 0.38 for nonantidromic, *t*-test, $P < 0.003$).

Differences in intrinsic properties of antidromic versus nonantidromic neurons

In addition to differences in the synaptic activation of these two classes of neurons, we sought to determine if there were differences in their intrinsic properties. To address this, we injected depolarizing and hyperpolarizing current pulses (±0.3, 0.5, 0.7, 1.0 nA lasting 500 ms) and measured the resultant membrane responses. The two classes of neurons had similar responses to hyperpolarizing current pulses but different responses to depolarizing current pulses. In general, the antidromic group was more excitable (Fig. 4); given the same magnitude of depolarizing pulse, they discharged more action potentials that were shorter in duration and each action potential was followed by smaller afterhyperpolarizations. ANOVA analysis between the two groups revealed that there were significant differences between the two groups based on physiological parameters [resting membrane potential, threshold for action potential initiation, rise and fall time of the action potential, action potential half-width at half-amplitude, magnitude and duration of the afterhyperpolarization, slope of the firing frequency vs. injected current curve (FI curve), input resistance, $P < 0.02$]. Subsequent post hoc analysis using *t*-tests was done to determine the source(s) of the variance. The firing rates of both neuronal populations were strongly correlated with the magnitude of the current pulses, $r^2 = 0.86 \pm 0.37$ for the antidromic group ($n = 14$) and $r^2 = 0.88 \pm 0.17$ for the nonantidromic group ($n = 10$). But the slopes of these functions were significantly different (Fig. 4, *C* and *D*), as the antidromic group had a steeper slope than the nonantidromic group (see Table 1).

We then investigated whether the differences in firing rates could be explained by differences in action potential dynamics. All 34 neurons that were physiologically characterized were found to be regular spiking neurons. For each neuron, action potential width at half-amplitude, and rise and decay times were determined (Fig. 4, *E* and *F*). Antidromic neurons had similar amplitudes but faster action potentials than nonantidromic neurons (Fig. 4*E*, Table 1). The half-width at half-amplitude was analyzed for the initial action potential in response to a depolarization that just exceeded threshold, and it was found that the antidromically activated neurons had significantly narrower action potentials. This difference in spike width could be accounted for by differences in the decay time of the action potential because there were no differences in the 10–90% rise times of the action potentials in the two groups (Fig. 4*F*, Table 1). Consistent with a faster repolarizing phase of the action potential, the time from the action potential peak amplitude to 90% of the peak afterhyperpolarization (AHP) was significantly faster in the antidromic neurons (see Table 1).

Not only were the antidromic neurons more excitable, they tended to rest at slightly more depolarized levels than their neighboring nonantidromic neurons, although this difference did not reach statistical significance (see Table 1). Similarly, action potential threshold was more hyperpolarized for antidromic neurons (Fig. 5*A*). Furthermore, the magnitude of the AHP (Fig. 5*B*) was significantly smaller in antidromic than the nonantidromic cells. Taken together these findings suggest that the antidromic neurons are more excitable.

The differences in excitability in the two populations could be due to a variety of factors including differences in channel expression or input resistance (see Larkman et al. 1992; Rall and Rinzel 1973). To test this, input resistance was computed in response to a small-magnitude (−0.3 nA) hyperpolarizing current pulse of 500-ms duration at three time points: 150 ms after pulse onset (after the RC transient), at the time of peak deflection, and at 450 ms, just prior to offset of the hyperpo-

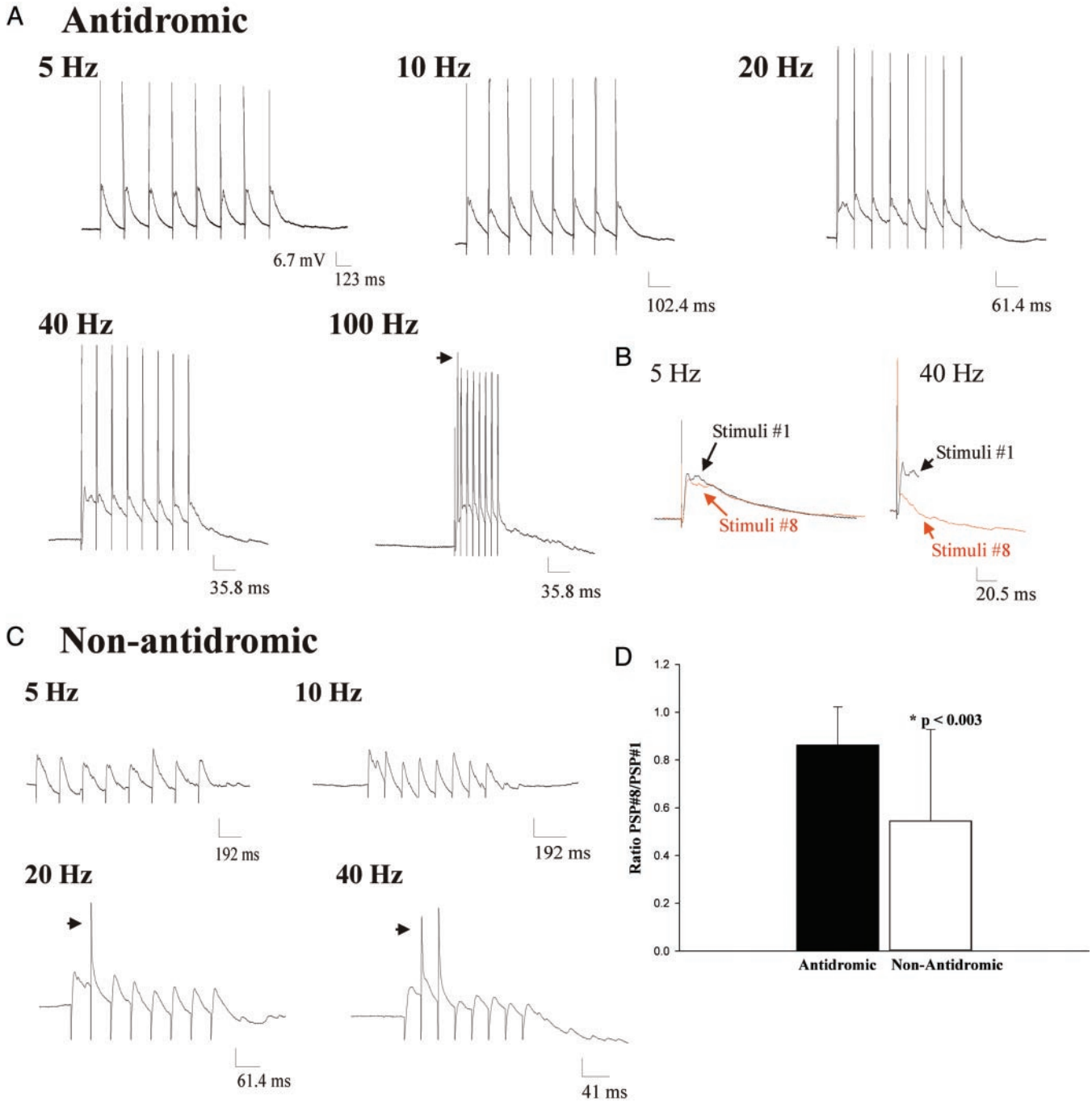

FIG. 3. Responses to different frequencies of white matter stimulation. *A*: antidromic neuron. Note that there is no action potential failure at any frequency, a hallmark of antidromic activity. At higher frequencies of stimulation, the feedforward synaptic input can exceed threshold and initiate an action potential (→ in response to 100-Hz stimuli). *B*: overlaying the 1st and 8th response at 5 and 40 Hz reveals that there is more synaptic depression at higher stimulation frequencies. *C*: response of a nonantidromic cell to white matter stimulation. Note that summation of synaptic input can evoke action potentials (→) in response to 20- and 40-Hz stimulation. *D*: the synaptic responses depress. The ratio of the magnitudes of the 8th synaptic response to the 1st when the white matter was stimulated at 5 Hz reveals that the nonantidromic neurons show significantly (*) greater depression. Plotted are the means ± 1 SD. Stimulus artifacts have been truncated. For all panels, the *y* axis is equivalent. Action potentials and stimulus artifacts have been truncated.

larizing pulse, to assess for the existence and magnitude of hyperpolarizing-activated cation currents (Fig. 5, *C* and *D*). Maximum input resistance for the antidromic neurons was lower but not significantly so when compared with the nonantidromic neurons. At each of the other two time points nonantidromic neurons had a higher input resistance, but these differences also did not reach statistical significance (*t*-tests, *P*s > 0.05). Furthermore, there were no statistical differences between the input resistances measured at the three different time points within the two groups (paired *t*-tests, *P*s > 0.05). Hyperpolarization-activated cation currents might not have been sufficiently activated by such a small current pulse, so to

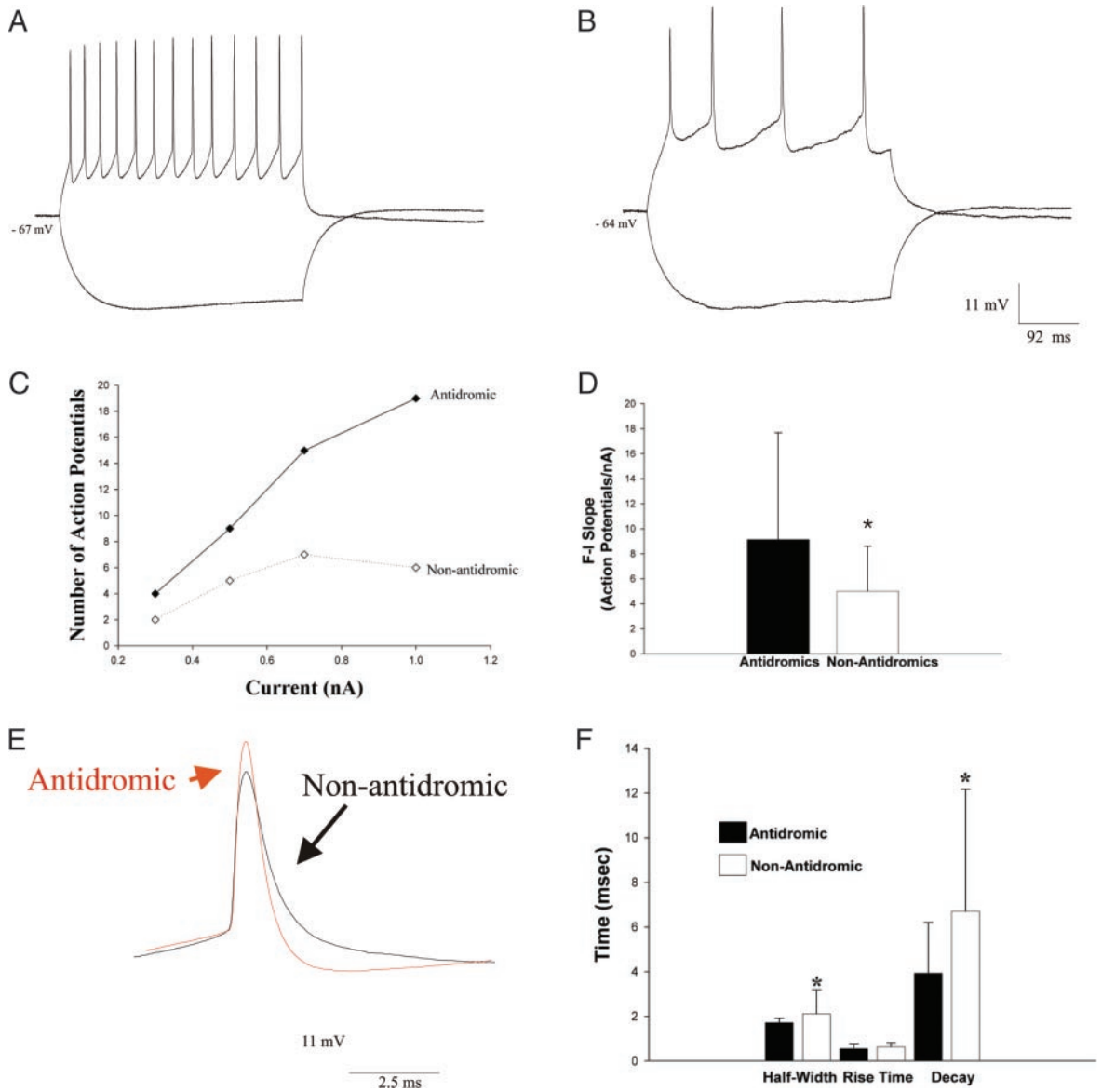

FIG. 4. Antidromic neurons are more excitable in response to depolarizing current pulses. Responses from an antidromically activated neuron (*A*) and a nonantidromically activated neuron (*B*) to ± 0.7-nA current pulses lasting 500 ms. Note the similar input resistances but the more robust response by the antidromic neuron. *C*: antidromic neurons were more excitable in response to depolarizing current pulses. Responses of an antidromic neuron (—) and a nonantidromic neuron (· · ·) reveal that the slope of the input/output curve in the antidromic neuron is steeper. *D*: population data confirms this difference ($*P < 0.05$). Plotted are the means ± SD. *E*: the action potentials of an antidromic and a nonantidromic neuron overlaid at spike threshold. *F*: the half-widths measured at half-amplitude were thinner for the antidromic neurons due to differences in the falling phase of the action potential (*F*, $*P < 0.05$). Plotted are means ± SD.

further test for their existence, 500-ms pulses of −0.5, −0.7, and −1.0 nA were delivered (Fig. 5*C*). Even with pulses of −1.0 nA, which resulted in the membrane potentials exceeding −100 mV in some cases, there were no statistical differences in the input resistance measured at the three time points (paired *t*-tests, *P*s > 0.05), providing little evidence for a strong role for hyperpolarization activated cation currents in layer VI neurons of either group. This finding is consistent with in situ hybridization data, showing little evidence for the presence of the hyperpolarizing-activated cation channel in mouse layer VI (Santoro et al. 2000). We concluded that antidromic neurons tend to rest closer to threshold and given similar input resistances, and they are more likely to fire in response to a depolarizing input.

Anatomical differences of between antidromic and nonantidromic neurons

Do the physiological differences observed in the two classes of neurons correlate with differences in morphology? To test this hypothesis, three-dimensional anatomical reconstructions of biocytin-filled neurons were undertaken. All 34 of the neurons studied physiologically were reconstructed. Antidromic neurons had a similar number of primary dendrites but had longer apical dendrites and less elaborate dendrites than the nonantidromic neurons (Figs. 6 and 7). Antidromic neurons had apical dendrites, which reached layer IV and, in some cases, layer II; in no case did their dendrites reach the pial surface and the size of their apical tuft was small compared

TABLE 1. *Action potential parameters*

Parameter	Antidromic Neurons	Non-antidromic Neurons
n	14	10
Resting membrane potential, mV	−67.0 ± 8.4	−70.2 ± 5.5
Slope of FI curve, action potentials/nA	9.1 ± 8.6	4.9 ± 3.6*
Action potential		
Threshold, mV	−39.3 ± 6.2	−32.1 ± 5.4*
Width at half amplitude, ms	1.7 ± 0.2	2.1 ± 1.1*
Rise time, ms	0.55 ± 0.2	0.63 ± 0.2
Fall time, peak to 90% of AHP, ms	3.9 ± 2.3	6.7 ± 5.5*
Magnitude of AHP, mV	8.8 ± 6.9	14.2 ± 2.8*
Maximum R_{in}, MΩ	456.9 ± 179.9	588.9 ± 167.8

Reported data are means ± SD. * *t*-test $P < 0.05$.

with layer V cortico-tectal neurons (Kozloski et al. 2001; Markram et al. 1997). On average, the apical dendrite of the antidromic neuron was longer than the nonantidromic neurons, but this difference did not reach statistical significance (*t*-test, $P > 0.05$), presumably due to an outlier in the nonantidromic population and clipping of several antidromic neurons' apical dendrites due to the slicing process. The distributions of the lengths of the apical dendrites of the two groups were different (χ^2 analysis, $P < 0.05$, Fig. 8*A*).

Although the antidromic and the nonantidromic neurons had similar numbers of primary dendrites (antidromic = 4.5 ± 1.6, nonantidromic = 4.3 ± 1.9, *t*-test, $P > 0.05$), nonantidromic neurons had more branch points (6.0 ± 5.6 vs. 2.3 ± 2.6) and had more dendritic ends (11.0 ± 5.7 vs. 5.7 ± 4.0) both of which are indicators of more nonprimary dendrites (Fig. 8*B*, *t*-test, $P < 0.05$). Further analysis showed that the nonantidromic neurons on average had similar numbers of secondary

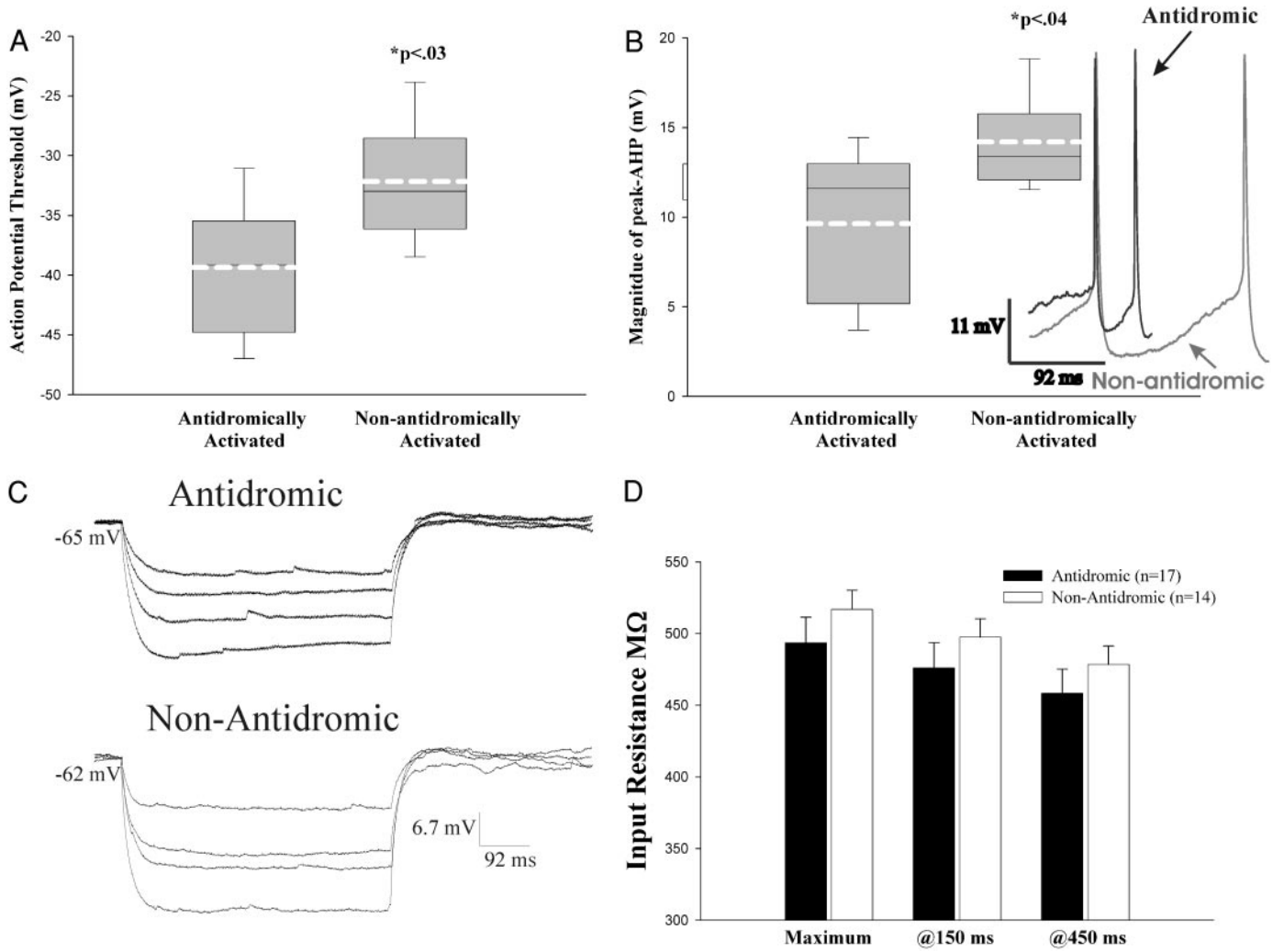

FIG. 5. Intrinsic properties of antidromic and nonantidromic neurons. *A*: box and whisker plots reveal that the action potential threshold for the antidromic neurons were hyperpolarized relative to those of the nonantidromic neurons. *B*: the magnitudes of the afterhyperpolarizations (AHPs) were larger in the nonantidromic population. *Inset*: a representative AHP for each population aligned to action potential threshold. For both box plots, the solid black line represents the median value, the white dashed line is the population mean, the box represents the 25–75% quartiles and the error bars represent the SDs. *C*: the input resistance of the antidromic neurons was similar to that of the nonantidromic neurons. Voltage traces are representative responses to 500-ms hyperpolarizing pulses of −0.3-, −0.5-, −0.7-, and −1.0-nA magnitudes. *D*: quantification of the input resistance at 3 time points revealed little evidence for hyperpolarization-activated cation currents and that the nonantidromic neurons tended to have greater input resistances, but none of these differences reached statistical significance. Plotted are the means ± SE.

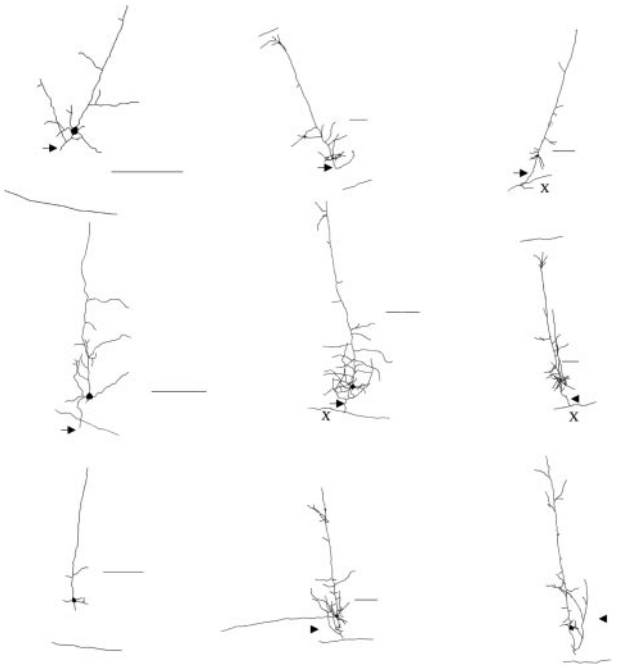

FIG. 6. Morphologies of antidromic neurons. Representative morphological reconstructions of antidromic neurons. Note the pyramidal cell bodies, axons that reach the white matter and the prominent apical dendrites. The — beneath each neuron is the white matter-layer VI border. →, axons; ×, the putative site of the stimulating electrode. Scale bars indicate 100 μm.

dendrites but had significantly (*t*-test, $P > 0.05$) more tertiary (4.9 ± 2.6 vs. 1.4 ± 4.1) and quaternary dendrites (1.1 ± 1.2 vs. 0 ± 0) than the neighboring antidromic neurons. In cases of incomplete fills, we counted all the observable branch points and thus have most likely underestimated this metric for both populations. Despite this limitation, nonantidromic cells had significantly greater dendritic length due to their larger number of non primary dendrites (Fig. 8*C*, *t*-test, $P < 0.05$).

Antidromic neurons also tended to be within a very limited zone in the white matter-pia axis (111.07 ± 33.99 μm from the white matter). This strata corresponds with the upper half of layer VI, which is where the corticothalamic neurons reside (see Zhang and Deschenes 1997). Antidromic neurons had axons that reached the white matter and, in some cases, could be traced back to the putative stimulation site, further supporting the physiological finding that these neurons were antidromically activated. Furthermore, antidromic neurons did not have axons that ramified extensively in layer VI, and when there was an axonal collateral, it appeared to be heading toward layer IV, a known target of layer VI pyramidal neurons (Katz 1987; Staiger et al. 1996). In no case (of 14) did a nonantidromic neuron have an axon that reached the white matter. In the cases where the axon of the antidromically activated neuron could be traced back to the site of stimulation ($n = 4$), we were able to calculate the axonal conduction velocity by measuring the axonal length and determining the latency of the antidromic action potential. The average conduction velocity was 2.44 ± 0.64 m/s, which is very similar to the 2.5 ± 1.5 m/s conduction velocity reported for corticothalamic units in vivo in rats (see DISCUSSION) and significantly slower than the reported conduction velocity of other corticofugal axons (5.9 ± 1.6 m/s) (Kelley et al. 2001).

Taken together with the physiological results detailed in the preceding text, we concluded that neurons that are antidromically activated following white matter stimulation compose a distinct class of neocortical neurons.

Most antidromic cells resemble cortico-thalamic neurons

Based on comparison of our results to those of previous studies, we believed that the antidromic neurons were corticogeniculate neurons (see Katz 1987; Staiger et al. 1996; Zhang and Deschenes 1997). To test this we injected rhodamine beads into the dLGN of PND 8–10 mice in vivo (Fig. 9*A*) and waited a minimum 3 days for retrograde transport back to the somata of layer VI neurons in V1 (Fig. 9*B*). Occasionally a second band of neurons was labeled in layer Va (data not shown) presumably due to retrograde transport from the vLGN (Ojima et al. 1996). This method thus allowed for the identification of cortico-geniculate neurons. Bead-labeled neurons were subsequently targeted for electrophysiological and morphological analysis (Fig. 9, *inset*).

Bead-labeled corticothalamic neurons were all classified as regular spiking ($n = 23$ of 23). Some neurons showed signs of hyperpolarizing-activated cation currents as an inward sag in response to the most hyperpolarizing current pulse (−1.0 nA, see Fig. 10*A*). However, similar to the antidromic population, there were no significant differences in the input resistance measured at the maximum voltage deflection in response to a hyperpolarizing pulse at either 150 or 450 ms after pulse onset. In response to depolarizing current pulses, they discharged relatively broad action potentials, measuring 2.33 ± 0.58 ms at half height ($n = 23$, see Fig. 10*B*). The FI curve generated by the corticothalamic neurons in response to 500-ms depolarizing current pulses (Fig. 10*C*) was similar to that observed in the antidromically activated population (Fig. 4*C*). The peak frequency in response to a +1.0-nA, 500-ms step pulse was 22 Hz

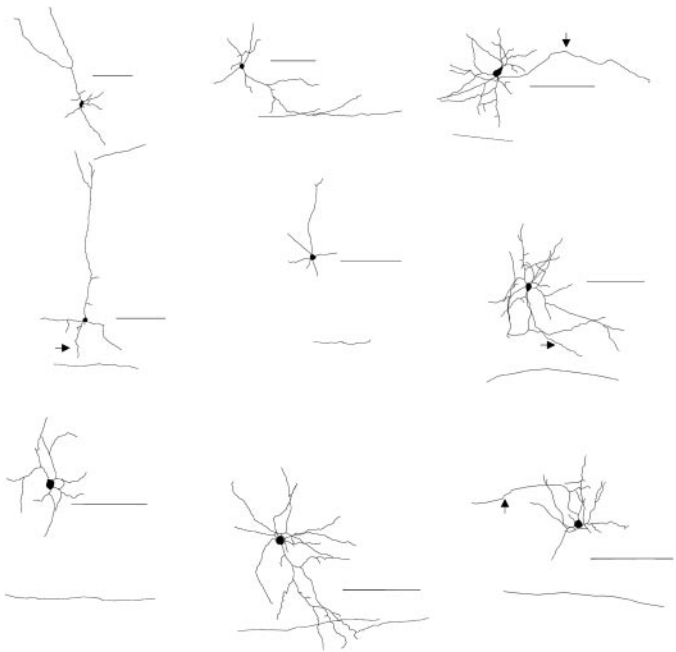

FIG. 7. Morphologies of nonantidromic neurons. Representative morphological reconstructions of nonantidromic neurons. Note the lack of apical dendrites and the nonpyramidal somata. The — beneath each neuron is the white matter-layer VI border. →, axons. Scale bars indicate 100 μm.

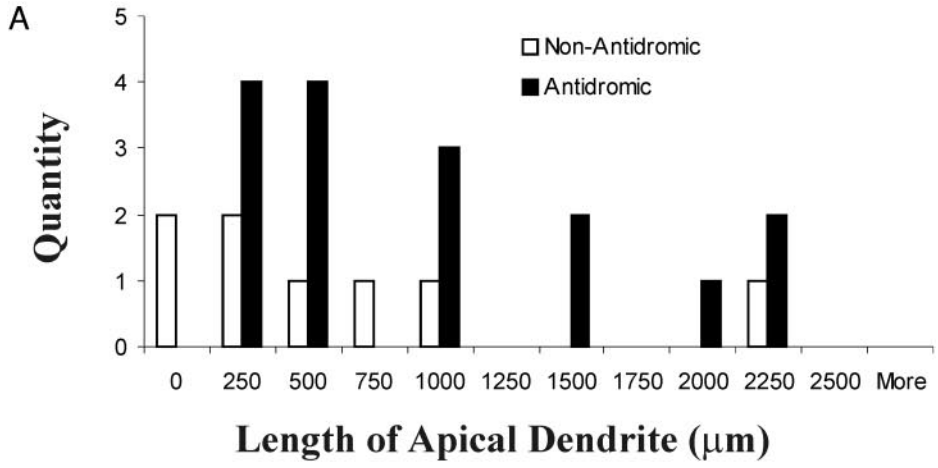

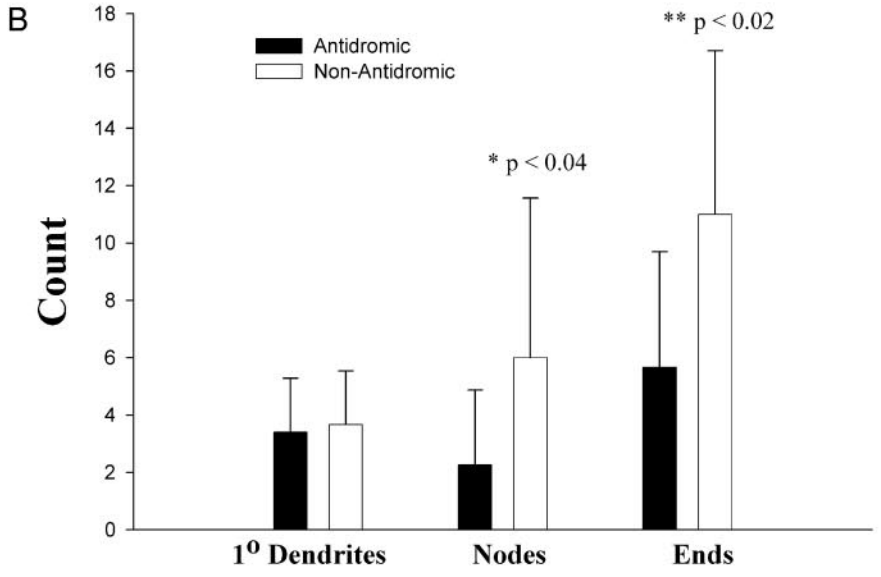

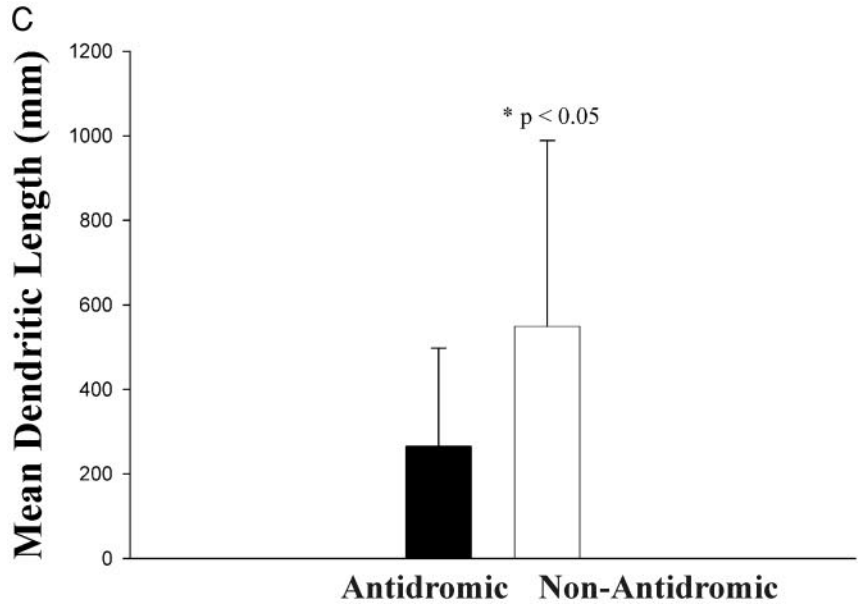

FIG. 8. Antidromic neurons have longer apical dendrites. *A*: histogram plotting the distribution of the lengths of apical dendrites in the 2 populations. *B*: antidromic neurons and nonantidromic neurons have similar numbers of primary dendrites, but nonantidromic neurons have more dendritic nodes and ends. *C*: the increased numbers of nonprimary dendrites lead the nonantidromic neurons to have longer dendritic trees. Plotted are means ± SD. * followed by *P* values represent statistical significance.

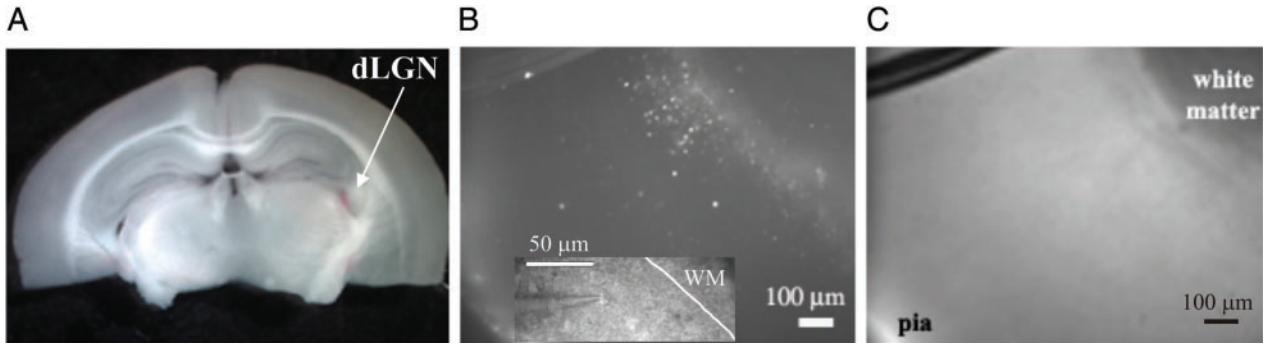

FIG. 9. Identification of cortico-geniculate neurons. Retrograde transport of rhodamine beads from the dorsal lateral geniculate nucleus of the thalamus (dLGN)–els a subpopulation of layer VI neurons. Rhodamine beads located in dLGN (*A*) are transported to cortico-geniculate neurons located in layer VI (*B*, compare with bright field image, *C*). These labeled neurons were then targeted for subsequent whole cell patch-clamp recordings (*inset*).

with the average being 5.3 ± 3.0 Hz ($n = 15$). Corticothalamic neurons showed little to no spike frequency adaptation in response to depolarizing current pulses (Fig. 10*D*). The average interspike interval from the 1st to the 10th interval was not significantly different (paired *t*-test, $P > 0.05$). Furthermore, in response to different intensity current pulses the interspike

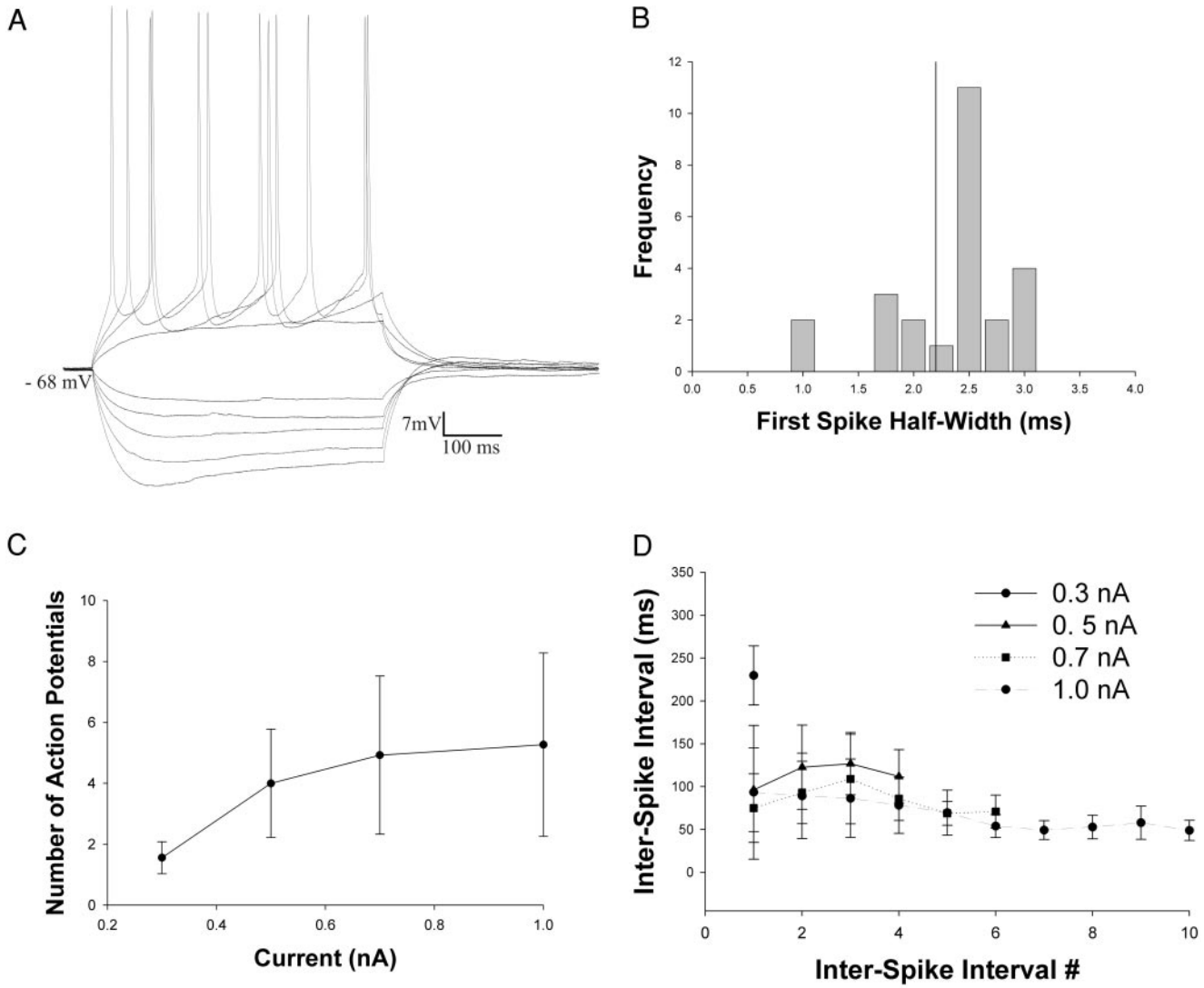

FIG. 10. Electrophysiological characterization of cortico-geniculate neurons. *A*: response of a typical cortico-geniculate neuron to a family of current pulses ±0.2-, 0.3-, 0.5-, 0.7-, 1.0-nA pulses lasting 500 ms. *B*: layer VI cortico-geniculate neurons discharged broad action potentials (single line represents population mean). Mean FI curve (*C*) and the lack of spike frequency spike adaptation (*D*) to 500-ms depolarizing current pulses are typical of cortico-geniculate neurons, means ± SD are plotted.

interval remained constant. Comparison of electrophysiological metrics (action potential amplitude, 10–90% rise time, decay time, resting membrane potential, action potential threshold, spike frequency adaptation, slope of FI curve, magnitude of the AHP, and input resistance) of the bead-labeled neurons with the antidromically activated neurons revealed no significant differences (*t*-test, $P > 0.05$). Similar analyses revealed that the identified cortico-geniculate neurons significantly differed from the nonantidromic neurons. Based on physiological measures, the bead-labeled cortico-geniculate neurons had taller and narrower action potentials than the nonantidromic neurons as well as having steeper FI curves and displaying less spike frequency adaptation (*t*-test, $P > 0.05$). These results suggest that the antidromic neurons and the bead-labeled cortico-geniculate neurons are derived from the same population of neurons.

Neocortical projection neurons are presumed to be pyramidal and, indeed, all bead-labeled cortico-geniculate neurons similar to the antidromic neurons were found to be pyramidal. Differential interference contrast images during the electrophysiological experiments already suggested a pyramidal shape (see Fig. 9, *inset*), and this was confirmed after recovering 6 of the 23 corticothalamic neurons and 3 of the 6 bead-labeled neurons recorded from layer Va (data not shown) all of which possessed pyramidal morphologies (Fig. 11). Corticothalamic neurons were characterized by pyramidal cell bodies and apical dendrites that gave rise to few oblique dendrites and appeared to lack apical tufts. Comparison between the morphologies of bead-labeled neurons and the antidromic neurons revealed no significant differences (*t*-test, $P > 0.05$); in soma size, soma shape (circularity index), soma perimeter, ratio of long to short somatic axis, number of primary dendrites, number of dendritic nodes, number of dendritic ends, and distance from the white matter. Furthermore, the nonantidromic neurons were found throughout layer VI, whereas the vast majority of the bead-labeled neurons were confined to one strata of layer VI. The two classes also differed in the mean size and shape of their soma with the cortico-geniculate neurons being larger and the nonantidromic neurons being rounder, the nonantidromic neurons also had significantly more dendritic nodes (*t*-test, $P < 0.05$). A further analysis was done using K-means clustering, a statistical algorithm that clusters cases (neurons) into different groups by seeking to minimize within group variance and maximize between group variance. Using all of the neurons where at least a partial biocytin fill was obtained and the corresponding physiological data, two groups were defined. One group contained all of the neurons pictured in Fig. 11 (bead-labeled cortico-geniculate neurons) and 12 of the 14 antidromically activated cells as well as 2 nonantidromic neurons, the second group contained 2 of 14 antidromically activated neurons and 8 of 10 nonantidromic neurons and no bead-labeled neurons. Based on these results, we propose that the antidromically activated neurons are indeed cortico-geniculate neurons and constitute a unique class of neocortical pyramidal neurons.

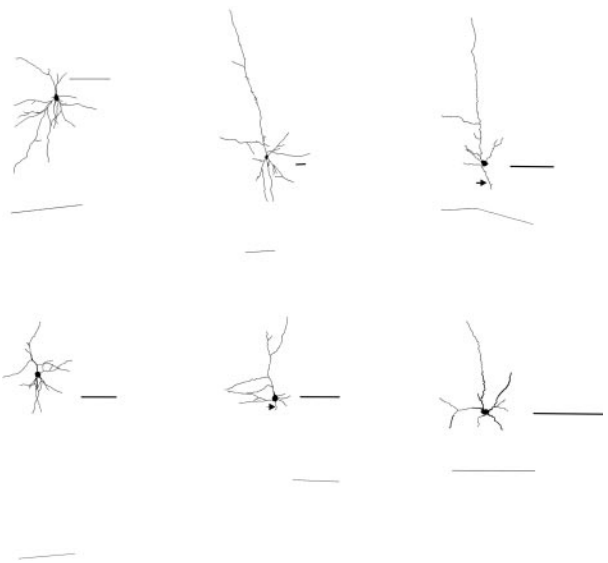

FIG. 11. Morphology of cortico-geniculate neurons. Note their prominent apical dendrites and pyramidal morphology that resembles the antidromic population (see Fig. 6). Scale bars represents 100 μm, →, axon, and — beneath each neuron, the layer VI-white matter border.

DISCUSSION

Different types of neurons in layer VI

Previous morphological studies have shown several classes of neurons in layer VI (Prieto and Winer 1999). Anatomical studies using the Golgi technique have defined in some cases up to eight distinct morphological classes in mouse layer VI (Ferrer et al. 1986a). Although some attempts have been made to correlate the morphological differences with either their physiology (but see Kang and Kayano 1994; van Brederode and Snyder 1992; Yang et al. 1996) or projection site (Katz 1987, Zhang and Deschenes 1997). In particular, there has been little previous work in layer VI to quantitatively characterize these neurons using either morphological or physiological criteria.

The results from the present study indicate that neurons in layer VI of mouse V1 can be divided into at least two classes based on their responses to white matter stimulation. Those neurons that respond with antidromic action potentials after white mater stimulation are different both physiologically and morphologically from their neighboring neurons. The antidromic neurons are more excitable and have longer apical dendrites. Based on comparisons to identified cortico-geniculate neurons, most antidromic neurons are likely to be cortico-geniculate neurons. The nonantidromic group represents a variety of neuronal classes, and if we had used further criteria besides antidromic activation those neurons might have been further subdivided.

The potential for incomplete fills and the disruption of the neuron's morphology due to the slicing procedure is an important caveat when analyzing our biocytin-filled neurons from in vitro slices. These factors might have contributed to our inability to find larger morphometric differences between the antidromic and nonantidromic groups. Nevertheless, the morphology of the antidromic group was characterized by pyramidal neurons with long apical dendrites and short basilar skirts (see Fig. 6). The nonantidromic neurons, however, were a mix of morphological phenotypes (pyramidal cells, inverted pyramidal cells, nonpyramidal cells, see Fig. 7), thus we believe that the differences between these groups are real.

Why do these two groups of neurons have different physiological properties? One possibility is that the differences in

physiology might be a result of their differences in morphology (Mainen and Sejnowski 1996). Nevertheless, we hypothesize that there is a difference in the channels that underlie the spiking properties of these two neuronal classes. There are several physiological properties that distinguish these two phenotypes: excitability, spike half-width, spike threshold and the magnitude of their AHPs. The difference in the spike width is accounted for by differences in the down stroke of the action potential, not the rise time, suggesting that Na^+ channels most likely do not account for this difference. Differences in K^+ channel density have been shown previously to affect excitability, spike width, and AHP characteristics (Rudy 1988). Indeed, previous research has shown that there are differences in AHP characteristics between two classes of pyramidal neurons in layer VI (Kang and Kayano 1994). Differences in K^+ channel expression have been shown to affect spike width and affect excitability (Martina et al. 1998). The simplest explanation that would account for all the physiological differences observed in the present study would be a difference in K^+ channel density or expression.

Identity of antidromic neurons

A limitation of the in vitro preparation is that, in general, long axonal connections are severed during the slicing process, thus making it difficult to determine the target of the projection from cortical pyramidal cells. This could lead to an underestimation of corticofugal neurons in our preparation. In another study of antidromic activity in the auditory cortex using nonoptical methods, ~3% of the neurons possessed antidromic activity (Rose and Metherate 2001), a similar percentage to what is estimated in the present study by counting the number of neurons that responded with changes in their optical signal in response to white matter stimulation as a percentage of Fura-labeled neurons. Although anatomical tracing studies have found much higher proportions of corticothalamic neurons (Zhang and Deschenes 1997), perhaps the low number of antidromically activated neurons reflects difficulties in activating the axons of the corticothalamic neurons. Two putative targets of layer VI corticofugal neurons are the thalamus and the claustrum (Katz 1987). It is unclear how many V1 neurons within the mouse project to the claustrum. In the rat, the bulk of the projection originates in V2 (Carey and Neal 1985; Sadowski et al. 1997). Furthermore, claustral projecting neurons have apical dendrites that reach layer I while the apical dendrites of corticothalamic neurons do not extend so superficially (Katz 1987). This is consistent with our present finding that the apical dendrites of antidromic neurons do not reach layer I. This, coupled with the lack of a strong projection to the claustrum from V1, suggests that the antidromic neurons are not cortico-claustral neurons.

Interestingly, synaptic inputs onto the antidromic neurons did not depress as much as those inputs onto nonantidromic neurons. Thalamocortical afferents show a preference for corticothalamic neurons in layer VI of the somatosensory cortex (White and Hersch 1982) and thalamocortical synapses in layer IV do not show as much depression as other local inputs (Amitai 2001), although thalamocortical synapses in layer VI do show some depression (Beierlein and Connors 2002). Comparing antidromic neurons to identified corticothalamic neurons in cat (Katz 1987) and rat (Bourassa and Deschenes 1995; Zhang and Deschenes 1997), it appears that they have similar morphological features: apical dendrites that do not reach layer I, axons that do not branch extensively in layer V and small to nonexistent apical tufts. Furthermore, when compared with identified cortico-geniculate neurons in mouse V1 in the present study, there were many similarities (see RESULTS). Additionally, the slow axonal conduction velocities of the antidromic neurons are consistent with previous reports of corticothalamic latencies in vivo. The reported mean of 2.44 m/s is within the range reported for corticothalamic neurons in a host of different cortical areas and species. As noted in the preceding text, the VPm projecting neurons of at S1 had a mean conduction velocity of 2.5 m/s (Kelly et al. 2001). In rabbit barrel cortex, corticothalamic neurons had mean conduction velocity of 1.6 m/s (range = 0.6–9.6 m/s) (Swadlow 1989). In cat striate cortex, three classes of cortico-geniculate neurons have been described based on their conduction velocities (Tsumoto and Suda 1980): slow (0.3–1.6 m/s), intermediate (3.2–11 m/s), and fast (13–32 m/s). In contrast, the cortico-geniculate neurons of the rabbit visual system appear to have slower conduction velocities [mean = 0.67 m/s (Swadlow and Weyand 1981); mean = 1.2 m/s (Swadlow and Weyand 1987)]. In both rabbit and cat, the cortico-callosal and -tectal axons have significantly higher conduction velocities than the cortico-geniculate neurons (Ferster and Lindstrom 1981; Harvey 1980; Swadlow and Weyand 1981; 1987). The lack of fast-conduction velocities in our sample might reflect our inability to stimulate these axons or that the mouse, like the rabbit, might not posses this class of cortico-geniculate axons. It is important to note that our measurements were made in vitro, and thus comparisons to in vivo results where ongoing activity and differences in temperature might effect conduction velocity could influence the comparison (Swadlow 1998). Based on similarities in physiology and anatomy, we conclude that the antidromic neurons in this study are largely corticothalamic neurons.

The physiological responses of cortico-geniculate and antidromically activated neurons were characterized by broad action potentials and nonadapting spike trains. Previous research has shown that layer VI neurons have broader action potentials than the pyramidal neurons in layer Vb (van Brederode and Snyder 1992); similar spike widths were observed in the present study, but their physiological significance is unclear. It is possible that a broad spike could depolarize the presynaptic bouton more efficiently. Synergistically, nonadapting spike trains could also serve to maximize the depolarization of the presynaptic terminal and thus increase the likelihood of synaptic release within the thalamus. Trains of cortico-geniculate action potentials have been shown to have a strong influence in the modulation of ongoing thalamic rhythms (Blumenfeld and McCormick 2000) and thus play an important role in gating information from the sensory periphery to the cortex (Guillery and Sherman 2002).

Thanks to G. Aaron, S. F. Brumberg, M. Beierlein, J. MacLean, H. Mansvelder, and C. Portera for helpful discussions and comments on the manuscript.

J. C. Brumberg was supported by National Institutes of Health Grant MH-01944-01, and the laboratory was supported by NIH Grant EY-11787.

REFERENCES

Amitai Y. Thalamocortical synaptic connections: efficacy, modulation, inhibition, and plasticity. *Rev Neurosci* 12: 159–173, 2001.

Beierlein M and Connors BW. Short-term dynamics of thalamocortical and intracortical synapses onto layer VI neurons in neocortex. *J Neurophysiol* 89: 1924–1932, 2002.

Blumenfeld H and McCormick DA. Corticothalamic inputs control the pattern of activity generated in thalamocortical networks. *J Neurosci* 20: 5153–5162, 2000.

Bourassa J and Deschnes M. Corticothalmic projections from the primary visual cortex in rats: a single fiber study using biocytin as an anterograde tracer. *Neurosci* 66: 253–263, 1995.

Brumberg JC, Nowak LG, and McCormick DA. Ionic mechanisms underlying repetitive high frequency burst firing in cortical neurons. *J Neurosci* 20: 4829–4843, 2000.

Burkhalter A. Intrinsic connections of rat primary visual cortex: laminar organization of axonal projections. *J Comp Neurol* 279: 171–186, 1989.

Carey RG and Neal TL. The rat claustrum: afferent and efferent connections with visual cortex. *Brain Res* 329: 185–193, 1985.

Chmielowska J, Carvell GE, and Simons DJ. Spatial organization of thalamocortical and corticothalamic projection systems in the rat SmI barrel cortex. *J Comp Neurol* 285: 325–338, 1989.

Eccles JC. *The Neurophysiological Basis of Mind.* Oxford, UK: Clarendon, 1952.

Erisir A, Van Horn SC, and Sherman M. Relative numbers of cortical and brain stem inputs to the lateral geniculate nucleus. *Proc Natl Acad Sci USA* 94: 1517–1520, 1997.

Ferrer I, Fabregues I, and Condom EA. Golgi study of the sixth layer of the cerebral cortex. I. The lisencephalic brain of Rodentia, Lagomorpha, Insectivora, and Chiroptera. *J Anat* 145: 217–234, 1986a.

Ferrer I, Fabregues I, and Condom EA. Golgi study of the sixth layer of the cerebral cortex. I. The gyrencephalic brain of Carnivora, Artiodactyla, and Primates. *J Anat* 146: 87–104, 1986b.

Ferster D and Lindstrom S. An intracellular analysis of geniculo-cortical connectivity in area 17 of the cat. *J Physiol* 342: 181–215, 1983.

Guillery RW and Sherman SM. Thalamic relay function and their role in corticocortical communication: generalizations from the visual system. *Neuron* 33: 163–175, 2002.

Harvey AR. A physiological analysis of subcortical and commissural projections of areas 17 and 18 of the cat. *J Physiol* 302: 507–534, 1980.

Jones EG. Laminar distribution of cortical efferent cells. *Cerebral Cortex, Cellular Components of the Cerebral Cortex* edited by Peters A and Jones EG. New York: Plenum, 1984, vol. 1, p. 521–553.

Kang Y and Kayano F. Electrophysiological and morphological characteristics of layer VI pyramidal cells in the cat motor cortex. *J Neurophysiol* 72: 578–591, 1994.

Katz LC. Local circuitry of identifies projection neurons in cat visual cortex brain slices. *J Neurosci* 7:1223–1249, 1987.

Kelly MK, Carvell GE, Hartings JA, and Simons DJ. Axonal conduction properties of antidromically identified neurons in rat barrel cortex. *Somat Mot Res* 18: 202–210, 2001.

Kozloski J, Hamzei-Sichani F, and Yuste R. Stereotyped position of local synaptic targets in neocortex. *Science* 293: 868–872, 2001.

Larkman AU, Major G, Stratford KJ, and Jack JJB. Dendritic morphology of pyramidal neurons of the visual cortex of the rat. IV. Electrical geometry. *J Comp Neurol* 323: 137–152, 1992.

Lorente de Nó R. Cerebral cortex: architecture, intracortical connections, motor projections. In: *Physiology of the Nervous System* (3rd. ed.), edited by Fulton JF. New York: Oxford, 1949, p. 288–330.

Mainen ZF and Sejnowski TJ. Influence of dendritic structure on firing pattern in model neocortical neurons. *Nature* 382: 363–366, 1996.

Markram H, Lubke J, Frotscher M, Roth A, and Sakmann B. Physiology and anatomy of synaptic connections between thick tufted pyramidal neurons in the developing rat neocortex. *J Physiol* 500: 409–440, 1997.

Martina M, Schultz JH, Ehmke H, Monyer H, and Jonas P. Functional and molecular differences between voltage-gated K^+ channels of fast-spiking interneurons and pyramidal neurons of rat hippocampus. *J Neurosci* 18: 8111–8125, 1998.

McCormick DA, Connors BW, Lighthall JW, and Prince DA. Comparative electrophysiology of pyramidal and sparsely spiny stellate neurons of the neocortex. *J Neurophysiol* 54: 782–806, 1985.

Mountcastle, VB. *Perceptual Neuroscience. The Cerebral Cortex.* Cambridge, Harvard Univ. Press, 1998.

Ojima H, Murakami K, and Kishi K. Dual termination modes of corticothalamic fibers originating from pyramids of layers 5 and 6 in cat visual cortical area 17. *Neurosci Lett* 2028: 57–60, 1996.

Prieto JJ and Winer JA. Layer VI in cat primary auditory cortex: Golgi study and sublaminar origins of projection neurons. *J Comp Neurol* 404: 332–358, 1999.

Rall W and Rinzel J. Branch input resistance and steady state attenuation for input to one branch of a dendritic neuron model. *Biophys J* 13: 648–688, 1973.

Rose HJ and Metherate R. Thalamic stimulation largely elicits orthodromic, rather than antidromic, cortical activation in an auditory thalamocortical slice. *Neuroscience* 106: 331–340, 2001.

Rudy B. Diversity and ubiquity of K channels. *Neuroscience* 25: 729–749, 1988.

Sadowski M, Morys J, Jakubowska-Sadowska K, and Narkiewicz O. Rat's claustrum shows two main cortico-related zones. *Brain Res* 756: 147–152, 1997.

Santoro B, Chen S, Luthi A, Pavlidis P, Shumyatsky GP, Tibbs GR, and Siegelbaum SA. Molecular and functional heterogeneity of hyperpolarization-activated pacemaker channels in the mouse CNS. *J Neurosci* 20: 5264–5275, 2000.

Sherman SM and Guillery RW. On the actions that one nerve cell can have on another: distinguishing "drivers" from modulators. *Proc Natl Acad Sci USA* 95: 7121–7126, 1998.

Staiger JF, Zilles K, and Freund TF. Recurrent axon collaterals of corticothalamic projection neurons in rat primary somatosensory cortex contribute to excitatory and inhibitory feedback loops. *Anat Embryol* 194: 533–543, 1996.

Swadlow HA. Efferent neurons and suspected interneurons in S-1 vibrissa cortex of the awake rabbit: receptive fields and axonal properties. *J Neurophysiol* 62: 288–307, 1989.

Swadlow HA. Neocortical efferent neurons with very slowly conducting axons: strategies for reliable antidromic identification. *J Neurosci Methods* 79: 131–141, 1998.

Swadlow HA and Weyand TG. Efferent systems of the rabbit visual cortex: laminar distribution of the cells of origin, axonal conduction velocities, and identification of axonal branches. *J Comp Neurol* 203: 799–822, 1981.

Swadlow HA and Weyand TG. Corticogeniculate neurons, corticotectal neurons, and suspected interneurons in visual cortex of awake rabbits: receptive-field properties, axonal properties, and effects of EEG arousal. *J Neurophysiol* 57: 977–1001, 1987.

Tombol T. Layer VI cells. In: *Cerebral Cortex: Cellular Components of the Cerebral Cortex*, edited by Peters A and Jones EG. New York: Plenum, 1984, p. 479–519.

Tsumoto T and Suda K. Three groups of cortico-geniculate neurons and their distribution in binocular and monocular segments of cat striate cortex. *J Comp Neurol* 193: 223–236, 1980.

Usrey M and Fitzpatrick D. Specificity in the axonal connections of layer VI neurons in tree shrew striate cortex: evidence for distinct granular and supragranular systems. *J Neurosci* 16: 1203–1218, 1996.

van Brederode JFM and Snyder GL. A comparison of the electrophysiological properties of morphologically identified cells in layers 5B and 6 of the rat neocortex. *Neuroscience* 50: 315–337, 1992.

White EL. *Cortical Circuits, Synaptic Organization of the Cerebral Cortex, Structure, Function, and Theory.* Boston, MA: Birkhauser, 1989.

White EL and Hersch SM. A quantitative study of thalamocortical and other synapses involving the apical dendrites of corticothalamic projection cells in mouse SmI cortex. *J Neurocytol* 11: 137–157, 1982.

Woodward WR, Chiaia N, Teyler TJ, Leiong L, and Coull BM. Organization of cortical afferent and efferent pathways in the white matter of the rat visual system. *Neuroscience* 36: 393–401, 1990.

Woodward WR and Coull BM. Localization and organization of geniculocortical and corticofugal fiber tracts within the subcortical white matter. *Neuroscience* 12: 1089–1099, 1984.

Yang CR, Seamens JK, and Gorelova N. Electrophysiological and morphological properties of layers V–VI principal pyramidal cells in rat prefrontal cortex *in vitro*. *J Neurosci* 16: 1904–1921, 1996.

Yuste R and Katz LC. Control of postsynaptic Ca^{2+} influx in developing neocortex by excitatory and inhibitory neurotransmitters. *Neuron* 6: 333–344, 1991.

Zhang Z-W and Deschenes M. Intracortical axonal projections of lamina VI cells of the primary somatosensory cortex in the rat: a single-cell labeling study. *J Neurosci* 17: 6365–6379, 1997.